DALTON

Stabilization of high oxidation states in transition metals. An electrochemical and computational study of structurally comparable molybdenum and tungsten complexes †

Klaus H. Moock,*[a] Stuart A. Macgregor,*[a] Graham A. Heath,[a] Sean Derrick[b] and René T. Boeré*[b]

[a] *Research School of Chemistry, Australian National University, Canberra ACT 0200, Australia*
[b] *Department of Chemistry, University of Lethbridge, Lethbridge, Alberta T1K 3M4, Canada*

Molybdenum and tungsten chlorides, chloride oxides and chloride nitrides as well as thiazene and phosphazene metallacycles were studied by electrochemical methods in CH_2Cl_2. The different ligand systems have a profound influence on the redox potentials. The stabilization of high valency increases from the hexachloro to pentachlorooxo to chloronitrido complexes and the metallacycles. There is a systematic difference in the electrode potentials between molybdenum and tungsten redox couples. The geometries of the d^1 and d^0 species, optimized using density functional methods, are in good agreement with the available experimental data and trends in redox data are reproduced by the computed energy difference between the appropriate d^1/d^0 pair. The relative stability of the higher oxidation state is directly linked to the donor properties of the ligands present, and increases in the order: $Cl_6 < F_6 < Cl_5O < Cl_4(N_3S_2) < Cl_3(N_3P_2) < Cl_4N$.

The chemistry of covalent early transition metals in high oxidation states is currently of intense interest. Organometallic chemistry was once associated exclusively with low-valent metals. However, research in the last decade has opened up a large and extensive organometallic chemistry involving metals in their highest oxidation state. The ability to bridge between traditional 'strong oxidizers' and easily oxidized organic species has relied on the ability of key 'spectator ligands' which greatly reduce the oxidizing power of the metals in such high oxidation states. Oxide, chloride, fluoride, η^5-C_5Me_5, and more recently imide are the most commonly employed ligands which possess the desired abilities, ranging from the traditional permanganate ion, in which four oxide ligands stabilize Mn^{VII}, to the exotic $(\eta^5\text{-}C_5Me_5)ReO_3$.[1] However, this important effect has rarely been quantified.

The obvious way to study the influence of ligand sets on redox potentials is by electrochemistry.[2] Traditional electrochemical investigations were performed in aqueous acid or alkali solutions, thereby ruling out many high-valent early transition-metal compounds, such as molybdenum and tungsten halide complexes, which are very sensitive to hydrolysis. There was therefore a need to perform systematic electrochemical investigations in typical organic solvents such as MeCN or CH_2Cl_2 to examine the influence of different ligand sets on the redox potentials for transition-metal complexes. Advances in electrochemical experimental techniques[3] in non-aqueous solutions made it possible to study the redox couples, $[MX_6]^{z/z-1}$, of a wide series of hexafluoro-[4] and hexachloro-metalates[5] of the second- and third-row transition metals. It has been recognized that these redox couples follow orderly trends which allow exact predictions of the redox stabilities for individual complexes. Such data present a parallel to the extensive electrochemical data for the elements in aqueous systems which are used in the construction of Latimer and Frost diagrams.[6]

Our approach has been to assemble a series of structurally similar, highly analogous metal complexes, based on octahedral or pseudo-octahedral geometry, in which the ligands are systematically varied. The parent species are the d^0 hexahalides $MoCl_6$ and WCl_6. We have varied only one or two of the chloride ligands by substitution by oxide, nitride and *cis*-diimide ligands {the latter derived from the novel inorganic chelates $[N_3S_2]^{3-}$ and $[N_3(PPh_2)]^{3-}$}.[7] The drastic lowering of the reduction potentials for the metal 6/5 and 5/4 redox couples that these ligand changes incur has been demonstrated. For this purpose we have chosen to conduct a comparative electrochemical study of the known molybdenum and tungsten complexes which will include data on the hexafluorides from a previous study: $[MoCl_6]^-$,[8] $[MoCl_6]^{2-}$,[9] WCl_6, $[WCl_6]^-$,[10] $[MoNCl_4]^-$,[11] $[WNCl_4]^-$,[11] $[MoF_6]^-$,[3a] $[WF_6]^-$,[3a] $[MoOCl_5]^{2-}$,[9] $[WOCl_5]^{2-}$,[9] $[MoCl_4(N_3S_2)]^-$,[12] $[WCl_4(N_3S_2)]^-$,[13] $[MoCl_3\{N_2(PPh_2)N\}]$,[14] and $[WCl_3\{N_2(PPh_2)_2N\}]$.[15] The structures of the redox-active anions in these salts are indicated in Fig. 1.

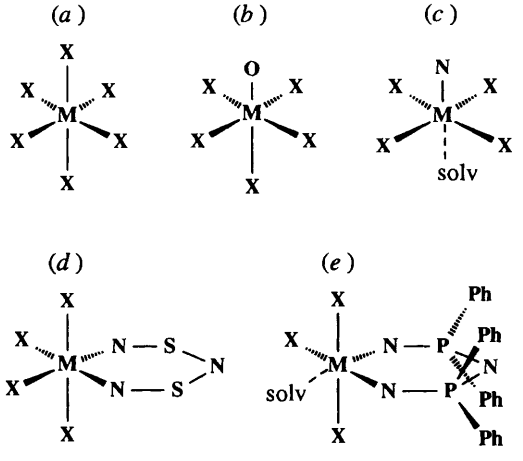

Fig. 1 Structures of the high-valent complexes studied

Of all the chlorometal complexes shown in Fig. 1 only the redox couples of $[WCl_6]^{z/z-1}$ ($z = 0, -1$ or -2) have been reasonably thoroughly investigated. In two independent studies

† *Supplementary data available* (No. SUP 59131, 21 pp.): optimized geometries. See Instructions for Authors, *J. Chem. Soc., Dalton Trans.*, 1996, Issue 1.

Non-SI unit employed: eV $\approx 1.60 \times 10^{-19}$ J.

carried out in MeCN[16] and CH_2Cl_2[17] the reported redox potentials are in good agreement with the potentials presented in this work. In an earlier study $[MoOCl_5]^{2-}$ {possibly in the form of $[MoOCl_4(MeCN)]^-$} was reduced in MeCN on a mercury electrode to an unknown molybdenum(III) species.[18] The electrochemistry of $[MF_6]^{z/z-1}$ (M = Mo or W; $z = 0$, -1 or -2) has been previously reported.[3,4] The only related nitrogen-containing systems studied by electrochemical methods have been the tungsten complexes $WCl_4Me(N{=}PPh_3)$, $WF_5(N{=}PPh_3)$ and $WF_4(N{=}PPh_3)_2$,[19] where the 'electronic stabilization' of the $Ph_3P{=}N$ ligand was recognized.

To support the electrochemical data and gain deeper insight into the electronic structure of the complexes we have undertaken a comprehensive computational study using density functional methods. Previously, one of us has successfully applied the X_α-SW (scattered wave) method to interpret the charge-transfer spectra of mono- and di-meric ruthenium halide species.[20] In this study we required more sophisticated density functionals which have been shown to reproduce molecular geometries accurately and allow reliable comparison of total energies.[21] Relatively few studies of systems containing metal centres in high oxidation states using this approach have been reported.[22] Given the utility of the density functional method in the study of low-oxidation-state transition-metal systems it is of interest to apply it to a different class of compounds. A number of *ab initio* studies on hexahalometalates have also appeared,[23,24] of which the study of the electron affinities of MF_6 and $[MF_6]^-$ (M = Mo or W) by Miyoshi and co-workers[23] is particularly relevant here.

The potential required to remove an electron is a reflection of the energy of the molecular orbital involved in the process and in this way electrochemical oxidation is related to an ionization process. Indeed a linear correlation between electrochemical oxidation data and vertical ionization energies has recently been found for a series of dithiadiazole radicals.[25] Electrochemical data also encapsulate contributions arising from changes in solvation and geometry. We cannot model such solvation changes with our present calculations, however, we can incorporate variations in geometry. In this study we aim to relate experimental redox data to computed differences in energy between the d^1 and d^0 systems at their optimized geometries. This calculated parameter will be referred to as an ionization energy, although strictly speaking it is the negative of a gas-phase electron affinity for the d^0 system involved. A preliminary report of some of this work has appeared.[26]

Results

Electrochemistry

All starting complexes studied for electrochemical work were found to be stable in a stringently purified CH_2Cl_2–NBu_4PF_6 solvent–electrolyte system. The more co-ordinating solvent MeCN can lead to substitution of chloride ligands from chlorometalate complexes as previously observed.[27] For electrochemical experiments over a temperature range of 223–298 K and at scan rates from 20 to 10 V s^{-1} the most effective inert electrolyte proved to be NBu_4PF_6. Electrode potentials were measured on a platinum working electrode using a special electrochemical cell described recently.[3a] All redox potentials are reported relative to the saturated calomel electrode (SCE) and are listed, together with the conditions of measurement, in Table 1.

$[NBu_4][MoCl_6]$, $[NBu_4]_2[MoCl_6]$, WCl_6 and $[NBu_4][WCl_6]$. The redox potentials for the hexachlorometalate systems have been independently obtained from two different starting oxidation states. For tungsten these were +6 and +5 and for molybdenum +5 and +4. Identical redox potentials were obtained from each starting complex. Three redox processes

Table 1 Voltammetric data for the compounds[a]

Compound	$E_{\frac{1}{2}}{}^b$/V $M^{6+/5+}$	$M^{5+/4+}$	$M^{4+/3+}$
$[NBu_4][MoCl_6]$	+2.20	+1.05	−0.28
$[NBu_4]_2[MoCl_6]$	+2.20	+1.05	−0.28
$[R]_n[MoF_6]$[c]	+2.04	+0.07	
$[NBu_4]_2[MoOCl_5]$	+1.70	−0.65[d]	
$[AsPh_4][MoCl_4(N_3S_2)]$	+0.62[e]	−0.68[f]	
$[MoCl_3\{N_2(PPh_2)N\}]$	+0.26	−0.67[g]	
$[AsPh_4][MoNCl_4]$	+0.25	−1.8[h]	
WCl_6	+1.59	+0.40	−1.15
$[NBu_4][WCl_6]$	+1.59	+0.40	
$[R]_n[WF_6]$[c]	+1.06	−0.93	
$[NBu_4]_2[WOCl_5]$	+0.95	−1.40	
$[AsPh_4][WCl_4(N_3S_2)]$	+0.09	−1.19[i]	
$[WCl_3\{N_2(PPh_2)N\}]$	−0.38	−1.50[i]	
$[AsPh_4][WNCl_4]$	−0.43	−2.48[j]	

[a] At a platinum electrode in CH_2Cl_2 containing 0.5 mol dm^{-3} NBu_4PF_6 electrolyte, referenced to SCE such that $E_{\frac{1}{2}} = +0.48$ V for $[Fe(\eta\text{-}C_5H_5)_2]^{+/0}$. [b] Reversible conditions at a scan rate $v = 100$ mV s^{-1} at 298 K, unless otherwise noted. [c] From ref. 3(a); potentials in MeCN, containing 0.1 mol dm^{-3} NBu_4PF_6 electrolyte, referenced to SCE such that $E_{\frac{1}{2}} = +0.38$ V for $[Fe(\eta\text{-}C_5H_5)_2]^{+/0}$. Average of the potentials of $[R]_n[MF_6]$, M = Mo or W, with $n = 1$ and R = $Fe(\eta\text{-}C_5H_5)(\eta\text{-}C_5H_4X)$, X = Br, I or $Fe(\eta\text{-}C_5H_4Br)_2$ and with $n = 2$ and R = $Co(\eta\text{-}C_5H_5)_2$·2MeCN. [d] Irreversible behaviour in cyclic voltammogram; quasi-reversible signal in a.c. experiment at −0.68 V. [e] Reversible process also confirmed by a.c. voltammetry. [f] Irreversible behaviour in cyclic voltammogram, $E_a = -0.8$ V; small signal in a.c. experiment at −0.68 V. [g] Quasi-reversible behaviour, separation of anodic peak (E_a) and cathodic peak (E_c), $E_a - E_c = 200$ mV, at $v = 500$ mV s^{-1} and 293 K. [h] Quasi-reversible behaviour $E_a - E_c = 200$ mV, at $v = 2$ V s^{-1} and 243 K. [i] Irreversible behaviour, E_a. [j] Reversible behaviour, $E_a - E_c = 58$ mV, at $v = 10$ V s^{-1} and 253 K.

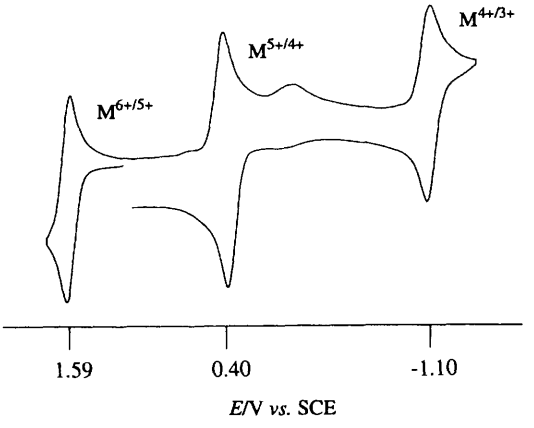

Fig. 2 Cyclic voltammogram of WCl_6 in CH_2Cl_2–$NBu^n_4PF_6$ starting from WCl_6. Three reversible redox couples are accessible for this metal complex

have been observed for both the chocolate brown, $4d^1$ $[NBu_4][Mo^VCl_6]$ and the yellow, $4d^2$ $[NBu_4]_2[Mo^{IV}Cl_6]$ complexes. The $[MoCl_6]^{-/2-}$ ($4d^1/4d^2$) and $[MoCl_6]^{2-/3-}$ ($4d^2/4d^3$) couples are reversible one-electron steps both in a.c. and d.c. modes, occurring at $E_{\frac{1}{2}} = +1.05$ and −0.28 V respectively. The oxidation step $[MoCl_6]^{-/0}$ ($4d^1/4d^0$) appears quasi-reversible and is observed at +2.20 V at 238 K. The salt $[NBu_4][MoCl_6]$ is very easily hydrolysed to give $[MoOCl_5]^{2-}$, the electrochemistry of which is also described below. The cyclic voltammogram of WCl_6 is shown in Fig. 2 and displays three redox couples. The $[WCl_6]^{0/-}$ ($5d^0/5d^1$) and $[WCl_6]^{-/2-}$ ($5d^1/5d^2$) reversible reductions occur at $E_{\frac{1}{2}} = +1.59$ and +0.40 V respectively. A further quasi-reversible reduction, $[WCl_6]^{2-/3-}$ ($5d^2/5d^3$), is seen at $E_{\frac{1}{2}} = -1.15$ V. While the first two processes have also been identified for $[NBu_4]$-$[W^VCl_6]$, the latter quasi-reversible reduction is obscured by

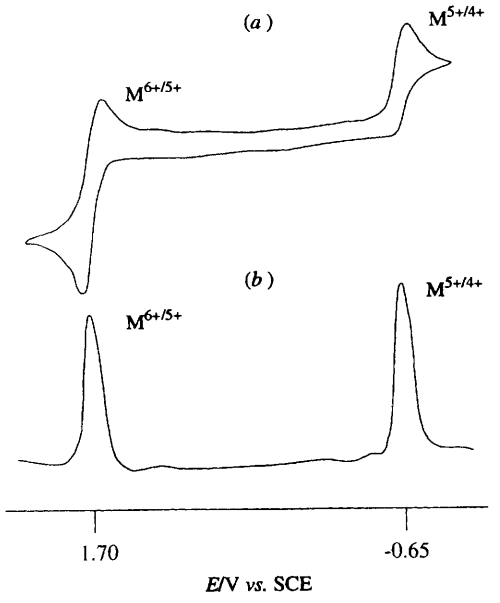

Fig. 3 Cyclic (*a*) and a.c. (*b*) voltammograms of the $[MoOCl_5]^{2-}$ complex ion, in CH_2Cl_2–$NBu^n_4PF_6$ solution

the presence of trace iodine from the synthesis of the compound.[10] Like the $[MoCl_6]^-$ complex, WCl_6 and $[WCl_6]^-$ are liable to hydrolyse to $[WOCl_5]^{2-}$.

$[NBu_4]_2[MoOCl_5]$ and $[NBu_4]_2[WOCl_5]$. The complex $[MoOCl_5]^{2-}$ contains a formal Mo=O double bond and has the electronic configuration $4d^1$. Metal-based oxidation to $4d^0$ $[MoOCl_5]^-$ and reduction to $4d^2$ $[MoOCl_5]^{3-}$ are therefore observed. Fig. 3 shows the cyclic and a.c. voltammograms of the complex at 293 K. The oxidation step $[MoOCl_5]^{2-/-}$ was reversible at $E_{\frac{1}{2}} = +1.70$ V in both scans. The reduction step $[MoOCl_5]^{2-/3-}$ was determined in the a.c. mode at $E_{\frac{1}{2}} = -0.65$ V. The cyclic voltammogram of this process shows no anodic return wave at 293 K and a scan rate of 100 mV s^{-1}. At faster scan rates (2 V s^{-1}) and lower temperatures (238 K) a return wave can be observed with a peak-current ratio, $i_{pc}:i_{pa}$, of 1:0.85. For $[NBu_4]_2[WOCl_5]$ ($5d^1$) a fully reversible one-electron oxidation process $[WOCl_5]^{2-/-}$ ($5d^1/5d^0$) at $E_{\frac{1}{2}} = +0.95$ V is observed. The reduction step $[WOCl_5]^{2-/3-}$ ($5d^1/5d^2$) appears quasi-reversible at -1.40 V (1 V s^{-1}, 238 K).

$[AsPh_4][MoNCl_4]$ and $[AsPh_4][WNCl_4]$. These complexes formally contain a metal–nitrogen triple bond, with both metals present in their highest formal oxidation state, VI ($4d^0$ and $5d^0$ respectively). Two redox couples have been detected for both systems. The first reduction, $[MNCl_4]^{-/2-}$, is a fully reversible one-electron step with $E_{\frac{1}{2}} = +0.25$ V (M = Mo, $4d^0/4d^1$) and -0.43 V (M = W, $5d^0/5d^1$). In the room-temperature cyclic voltammogram at slower scan rates (100 mV s^{-1}) the second reduction, $[MNCl_4]^{2-/3-}$, is chemically irreversible for both systems. Fig. 4 shows the cyclic voltammogram of $[AsPh_4]$-$[MoNCl_4]$ under these conditions. Faster scan rates and lower temperatures resulted in a quasi-reversible electrochemical response at $E_{\frac{1}{2}} = -1.8$ V (M = Mo, $4d^1/4d^2$, $v = 500$ mV s^{-1}, $T = 223$ K) and -2.48 V (M = W, $5d^1/5d^2$, $v = 10$ V s^{-1}, $T = 253$ K). Since both metal complexes are present in the nd^0 electronic configuration no oxidation processes are observed.

$[AsPh_4][MoCl_4(N_3S_2)]$ and $[AsPh_4][WCl_4(N_3S_2)]$. These metallacyclic complexes contain the N,N′-bidentate dithiatriazene moiety, $[N_3S_2]^{3-}$, with both molybdenum(VI) and tungsten(VI) in a formally nd^0 electronic configuration. Two reduction processes have been observed for these systems. The first reduction of $[AsPh_4][MCl_4(N_3S_2)]$ (M = Mo or W)

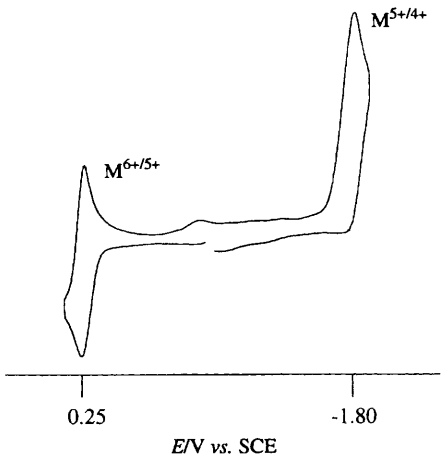

Fig. 4 Cyclic voltammogram of the $[MoNCl_4]^-$ complex ion, in CH_2Cl_2–$NBu^n_4PF_6$ solution

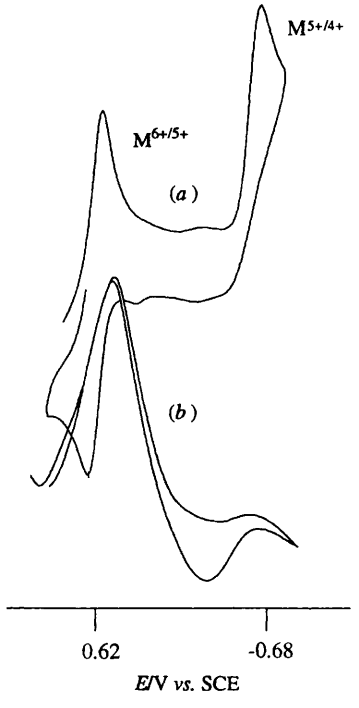

Fig. 5 Cyclic (*a*) and a.c (*b*) voltammograms of the $[MoCl_4(N_3S_2)]^-$ complex ion, in CH_2Cl_2–$NBu^n_4PF_6$ solution. The irreversibility of the +5/+4 couple is confirmed by the a.c. response

is a fully reversible metal-based one-electron step, $[MCl_4(N_3S_2)]^{-/2-}$ (nd^0/nd^1). The half-wave potential is observed at $E_{\frac{1}{2}} = +0.62$ (Mo) and +0.09 V (W). The second reduction is chemically and electrochemically irreversible for both metal complexes. Associated anodic waves occur at $E_a = -0.8$ V for the molybdenum complex and at -1.19 V for the tungsten analogue. Fig. 5 shows the cyclic and a.c. voltammograms of $[AsPh_4][MoCl_4(N_3S_2)]$ at room temperature. No oxidation processes could be observed for either metallacycle within the limit of solvent stability. Metal complexation clearly stabilizes the thiazene ring against oxidation as main-group dithiatriazenes are readily oxidized by Cl_2, $PhICl_2$ or XeF_2.[28]

$[MoCl_3\{N_2(PPh_2)_2N\}]$ and $[WCl_3\{N_2(PPh_2)_2N\}]$. The cyclic voltammogram of the $[WCl_3\{N_2(PPh_2)_2N\}]$ metallacycle in CH_2Cl_2 displays two one-electron steps, corresponding to the metal-centred d^0/d^1 and d^1/d^2 couples.[26] The first reduction is a fully reversible process at $E_{\frac{1}{2}} = -0.38$ V while the second has been identified as a chemically irreversible but electrochemically quasi-reversible step at $E_{\frac{1}{2}} = -1.5$ V. No oxidation steps have

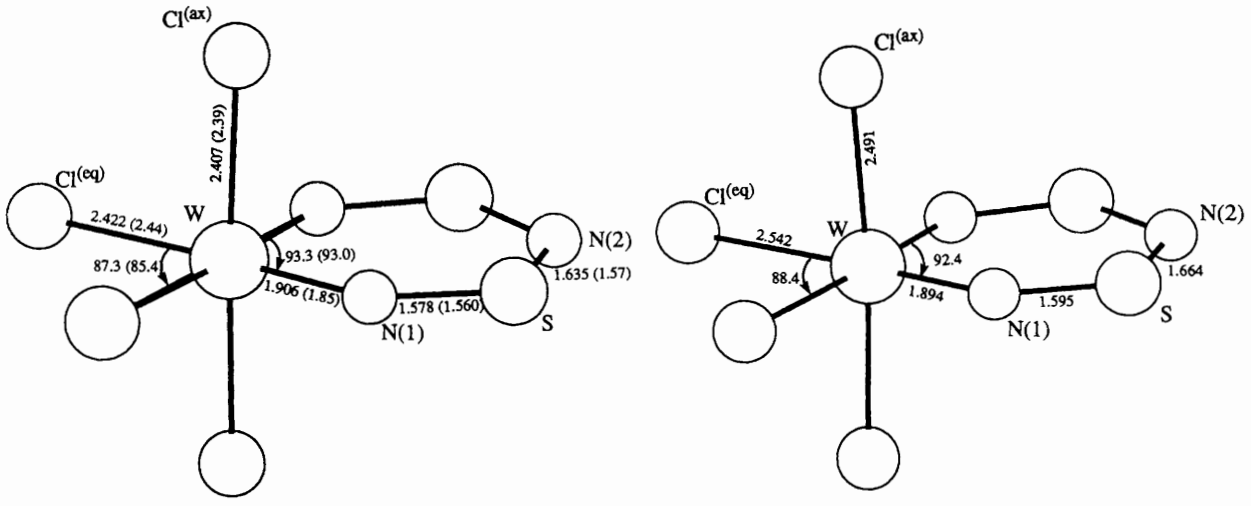

Fig. 6 Selected optimized bond distances (Å) and angles (°) for $[WCl_4(N_3S_2)]^-$ and $[WCl_4(N_3S_2)]^{2-}$. Average experimental parameters are given in parentheses where available.[12,35] Equivalent data for $[MoCl_4(N_3S_2)]^-$: Mo–Cl^{ax} 2.378 (2.404), Mo–Cl^{eq} 2.364 (2.444), Mo–N(1) 1.922 (1.836), N(1)–S 1.573 (1.565) and N(2)–S 1.640 (1.601 Å); Cl^{eq}–Mo–Cl^{eq} 88.3 and N(1)–Mo–N(1) 92.7 (92.6°). Selected optimized parameters for $[MoCl_4(N_3S_2)]^{2-}$: Mo–Cl^{ax} 2.434, Mo–Cl^{eq} 2.454; Mo–N(1) 1.893, N(1)–S 1.591 and N(2)–S 1.667 Å; Cl^{eq}–Mo–Cl^{eq} 88.7 and N(1)–Mo–N(1) 92.1°

been observed within the limits of solvent stability. For $[MoCl_3\{N_2(PPh_2)_2N\}]$ the first reduction process ($4d^1/4d^0$) is reversible at $E_{\frac{1}{2}} = +0.26$ V and the second reduction ($4d^2/4d^1$) is quasi-reversible at $E_{\frac{1}{2}} = -0.67$ V. No oxidation process was observed as expected for a metal in its highest oxidation state.

Optimized geometries

Geometry optimization was performed in the highest appropriate symmetry: O_h for $[MX_6]^{0/-}$ systems, C_{4v} for oxo- and nitrido-species and C_{2v} for $[MCl_4(N_3S_2)]^-$. Such d^1 $[MX_6]^-$ species are in principle subject to a Jahn–Teller distortion, however this effect is expected to be small.[29] Optimized distances for $[MX_6]^{0/-}$ species are given in Table 2 and compared with experimental data where available. Calculated geometric parameters for the oxo- and nitrido-species are given in Table 3 and those for $[MCl_4(N_3S_2)]^{2-/-}$ are detailed in Fig. 6. We have chosen not to optimize geometries for the phosphazene metallacycle because the precise nature of the species in solution is unclear (see below).

Computed ionization energies

Computed ionization energies and d^1/d^0 oxidation potentials are compared in Table 4 and plotted against one another in Fig. 7 for molybdenum. For a given metal the computed trends are good with the exception of the data for the chloride oxides. Whether the chloride oxide presents a specific problem for the present computational method is not clear. Further studies underway on related compounds will yield more information on the general applicability of our computational approach.[36] Previous theoretical studies on the gas-phase electron affinities of MF_6 (the negative of our computed ionization potentials) have produced a range of values. However, the calculated electron affinity has been consistently computed to be larger (*i.e.* more stabilizing) for Mo than W.[23,37] Our calculations repeat this trend with, here, the ionization energy of $[MoF_6]^-$ being slightly higher than that for $[WF_6]^-$ (by 0.27 eV). Trends in the experimental data reported for MF_6 electron affinities are not so clear-cut, overall suggesting only a small difference between the molybdenum and tungsten systems.[38]

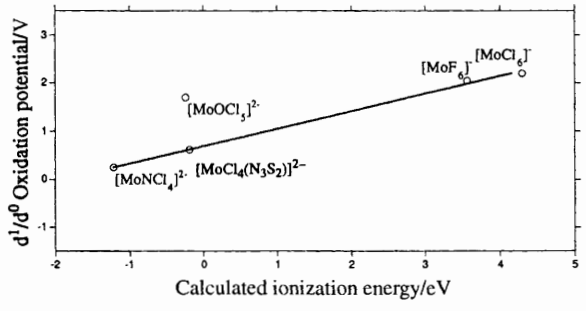

Fig. 7 Plot of calculated ionization energies *vs.* experimental oxidation potentials

Discussion

Structure and chemical identity of the complex anions

The complexes all have octahedral or pseudo-octahedral geometry (Fig. 1). The hexahalometalates, $[MX_6]^z$ (M = Mo or W; X = Cl or F; $z = 0, 1-$ or $2-$), belong to the point group O_h, and are close to regular octahedra for the hexachloro-[39] as well as for the hexafluoro-complexes.[23,39] With a single oxide ligand present, both neutral species $MOCl_3$ and $MOCl_4$ as well as the anionic $[MOCl_5]^{2-}$ (M = Mo or W) are chemically available.[40] Of these, the pentachloro-species is the most convenient to handle in solution and also maintains as similar a geometry as possible to the parent hexachloride. The pseudo-octahedral C_{4v} geometry of this anion has been established.[27] With a single nitride ligand present, both five-co-ordinate $[MNCl_4]^-$[11] and six co-ordinate $[MNCl_5]^{2-}$[41] are known. However, due to the insolubility of the latter, only $[MNCl_4]^-$ is suitable for electrochemical investigations. The $[MoNCl_4]^-$ anion has a C_{4v} square-pyramidal structure and shows clear indications of long secondary MN ··· M contacts in the solid state.[42] We therefore assume that in solution there will be a weakly co-ordinated species (solvent molecule or electrolyte anion) occupying the sixth co-ordination site, as indicated in Fig. 1(*c*). The metalladithiatriazenes of both molybdenum and tungsten are known in the neutral and anionic forms. The neutral forms are dimeric with two bridging chloride ligands.[35] This weak chloride bridge is broken by $AsPh_4Cl$, to form

Table 2 Calculated and experimental M–X distances (Å) for hexahalide species

	M = Mo		M = W	
Compound	Calculated	Experimental	Calculated	Experimental
MF_6	1.856	1.820[a]	1.898	1.831[b]
$[MF_6]^-$	1.912	*c*	1.954	*c*
MCl_6	2.309	*c*	2.360	2.24[d]
$[MCl_6]^-$	2.348	2.25[e]	2.400	2.33[f]

[a] Ref. 30. [b] Ref. 31. [c] Not available. [d] Ref. 32. [e] Mo–Cl axial bond in Mo_2Cl_{10}, ref. 33. [f] Ref 34.

Table 3 Calculated distances (Å) and angles (°) for $[MLCl_5]^{-/2-}$ (L = O) and $[MLCl_4]^{-/2-}$ (L = N; M = Mo or W)

Compound	M–L	M–Cl_{trans}	M–Cl_{cis}	L–M–Cl_{cis}
$[MoOCl_5]^-$	1.725	2.417	2.345	93.1
$[MoOCl_5]^{2-}$	1.722	2.498	2.417	93.4
$[WOCl_5]^-$	1.727	2.497	2.365	93.4
$[WOCl_5]^{2-}$	1.738	2.602	2.468	93.5
$[MoNCl_4]^-$	1.662		2.350	103.1
$[MoNCl_4]^{2-}$	1.671		2.438	104.9
$[WNCl_4]^-$	1.676		2.382	102.6
$[WNCl_4]^{2-}$	1.703		2.504	104.4

Table 4 Comparison of experimental oxidation potentials and calculated ionization energies

	M = Mo		M = W	
Compound	$E_{\frac{1}{2}}^{ox}$/V	E_i/eV	$E_{\frac{1}{2}}^{ox}$/V	E_i/eV
$[MCl_6]^-$	+2.20	+4.30	+1.59	+4.15
$[MF_6]^-$	+2.04	+3.56	+1.06	+3.29
$[MOCl_5]^{2-}$	+1.70	−0.24	+0.95	−0.25
$[MCl_4(N_3S_2)]^{2-}$	+0.62	−0.19	+0.09	−0.12
$[MNCl_4]^{2-}$	+0.25	−1.22	−0.43	−1.29

$$ML_x(d^0) \underset{-e}{\overset{+e}{\rightleftharpoons}} ML_x(d^1) \underset{-e}{\overset{+e}{\rightleftharpoons}} ML_x(d^2)$$

Scheme 1 M = Mo or W; L_x = F_6, Cl_6, Cl_5O, Cl_4N, $Cl_4(N_3S_2)$ or $Cl_3[N_2(PPh_2)_2N]$

$[AsPh_4]^+$ salts of the six-co-ordinate complexes, $[MCl_4(N_3S_2)]^-$, as indicated in Fig. 1(*d*).[12,35] In contrast, the neutral metallaphosphazenes are monomeric species, $[MCl_3\{N_2(PPh_2)_2N\}]$ (M = Mo or W). Their structure has been established as derived from a trigonal bipyramid with the three chlorides in a C_{3v} arrangement.[14] All our attempts to add Cl^- to these species, using, for example, $AsPh_4Cl$, were in vain, so that a structure directly comparable to the metalladithiatriazenes could not be obtained. However, the structure of an acetonitrile adduct of $[WCl_3\{N_2(PPh_2)_2N\}]$ has been determined by an X-ray study,[14] and is pseudo-octahedral as indicated in Fig. 1(*e*). We therefore assume that the metallaphosphazene complex will be weakly solvated in the electrolyte solution and possesses the indicated geometry. This discrepancy in structure between the metalladithiatriazenes and phosphazenes indicates a significantly stronger *trans* influence in the latter, which ought to be reflected in the redox chemistry (see below).

Ligand influence on redox stability

The present work provides the most comprehensive electrochemical study to date of a series of highly sensitive, high-valent molybdenum and tungsten complexes. From the redox potentials obtained (Table 1), the following observations arise.

(1) Two successive metal-centred redox processes linking molybdenum and tungsten in their respective d^0, d^1 and d^2 electronic configurations could be observed for all metal complexes studied (see Scheme 1). All the d^0/d^1 couples exhibit either full or close to full electrochemical reversibility, indicating the stability of the metals in both oxidation states under the conditions studied. The d^1/d^2 couples are, with exception of the hexachlorometalates, generally less reversible. This is probably due to an enhanced tendency to expel Cl^- in the reduced forms of the O- and N-containing complexes.

(2) The co-ordination environment as well as the oxidation state of the metal has a profound influence upon the potentials. Hence the redox couples cover a wide range for molybdenum from +2.20 V for $[MoCl_6]^{0/-}$ to −1.80 V for $[MoNCl_4]^{2-/3-}$ and for tungsten from +1.59 V for $[WCl_6]^{0/-}$ to −2.48 V for $[WNCl_4]^{2-/3-}$.

(3) For all electronic configurations studied (d^0, d^1 and d^2) the ligand array, L_x, stabilizes the metal centres at lower potentials according to the series: $Cl_6 < F_6 < Cl_5O < Cl_4(N_3S_2) < Cl_3(N_3P_2) < Cl_4N$. The stabilizing effect of fluoride relative to chloride has been recognized earlier.[5] For the chloro-complexes, WCl_6 and $MoCl_6$[43] are the strongest oxidizing agents of the tungsten and molybdenum series involving the d^0/d^1 redox step. The oxide ligand in $[MOCl_5]^{-/2-}$ lowers the potential of the d^0/d^1 step relative to MCl_6, which is further lowered by the nitride ligand in $[MNCl_4]^{-/2-}$. The overall effect of the cyclic, bidentate, nitrogen ligands in the metallacycles is similar to that of a single nitride ligand. The trend O < S < NPh has been determined for a series of molybdenum(v) complexes.[2]

(4) Successive redox couples for the same ligand array are separated by a constant value, these being 1.15/1.17 V for $[MCl_6]^{0/-}$–$[MCl_6]^{-/2-}$, 2.35 V for $[MOCl_5]^{-/2-}$–$[MOCl_5]^{2-/3-}$ and 2.05 V for $[MNCl_4]^{-/2-}$–$[MNCl_4]^{2-/3-}$ These separations are independent of the metal centre.

(5) The ring systems in the metallacycles stabilize the metals considerably, however, the potentials of the metal phosphazenes are approximately 0.4 V more negative than those of the dithiatriazene analogues. This, and the observation that a fourth Cl^- ligand cannot bind to the phosphazene complex, suggests the metal centre in this species is more electron rich compared to that in the other metallacycle.

(6) The molybdenum redox couples are systematically to higher positive potentials than their tungsten analogues. This shift in potential is 1.0 V for the fluoro-compounds[4b] and ranges from 0.53 $\{[MCl_4(N_3S_2)]^{-/2-}\}$ to 0.87 V ($[MCl_6]^{2-/3-}$). This difference has been observed before[5] and interpreted as a relativistic effect.[44]

(7) Only the hexachlorometalates have three redox processes within the accessible solvent window due to both the high positive potentials of the $[MCl_6]^{0/-}$ couple and the smaller separation between subsequent reductions.

(8) We have not been able to compensate for any effect of the overall charge on different complex ions on the redox potentials. However, it is gratifying that the potentials of the hexachlorometalates measured independently from species of different charge ($[MoCl_6]^-$ and $[MoCl_6]^{2-}$ as well as WCl_6 and $[WCl_6]^-$) are the same.

Optimized geometries

The optimized M–X distances for MX_6 and $[MX_6]^-$ species (Table 2) are consistently too long when compared to those determined experimentally. This effect has been found in other high-valent transition-metal systems containing similar π-donor ligands.[22] This contrasts with bond lengths calculated using the local-density approximation between soft ligands (*e.g.* CO and PR_3) and low-valent metal centres where the M–L bond distance is generally underestimated by between 0.05 and 0.1 Å.[21] Our computed results are similar to those of *ab initio* configuration-interaction calculations on the hexafluorides of Mo and W in which the computed M^{VI}–F distance was 1.881 Å for both Mo and W and the M^{V}–F distances were 1.936 and 1.937 for Mo and W respectively.[23]

Of the oxo- and nitrido-species (Table 3), direct comparison with crystallographic data is possible only for the $[MoNCl_4]^{-/2-}$ pair {Mo–N 1.66, Mo–Cl 2.345 Å and N–Mo–Cl 101.5° in $[MoNCl_4]^-$;[35] Mo–N 1.634, Mo–Cl 2.40 Å and N–Mo–Cl 100° in $[MoNCl_4]^{2-}$[45]}. The geometries of the metal(VI) nitrido-species have also been obtained using *ab initio* calculations (MP2 level) and similar structures were obtained.[22g] For the other species, comparison with related compounds suggests our calculated geometries are reasonable. Average geometric parameters for $[MoOCl_4(H_2O)]^-$ are Mo=O 1.665, Mo–Cl 2.364 Å and O=Mo–Cl 98.2° (two molecules per unit cell).[46] The W–N distance in $[WCl_5N(C_2Cl_5)]^-$ is 1.68 Å while $W–Cl_{cis}$ distances average 2.327 Å. The $W–Cl_{trans}$ bond is somewhat longer at 2.420 Å.[47] This *trans* lengthening is seen in the computed structures of the chloride oxides. The W=O distance in $[WOCl_4(ON_2Ph_2)]$ is 1.669 Å and W–Cl distances average 2.295 Å; O=W–Cl angles are all less than 90°, presumably a result of the influence of the azoxybenzene moiety.[48] Overall, calculated bond distances again tend to be overestimated compared to the experimental values. The M–Cl bond distances are longer for M = W than M = Mo. All M–Cl distances are significantly longer in the d^1 species, although changes in the M–O and M–N distances are minor between the d^0 and d^1 species. This is also seen in the crystal structures of the $[MoNCl_4]^{-/2-}$ pair where the Mo–N distance is actually shorter in the d^1 system. The extra electron occupies an orbital lying in the MCl_4 plane (see below), disrupting the M–Cl π interaction. The subsequent M–Cl lengthening reduces donation to the metal centre within the $\{MCl_4\}$ pseudo-plane. This loss of electron density at the metal may be compensated for by an increase in donation from the axial ligands with a shortened or unchanged M–N or M–O bond as a consequence. The calculated structure of $[WCl_4(N_3S_2)]^-$ is in good agreement with that determined crystallographically (Fig. 6).[35] Significant elongation of both the axial and equatorial W–Cl bonds is again found in the d^1 system, although the W–N bond shortens slightly in the lower oxidation state. Trends in the molydenum analogues are similar.

Comparison of computational results with E° data

With the exception of the chloride oxide species, Fig. 7 shows that the trends in redox data for a given metal are well reproduced by the calculated ionization energies. Even for the chloride oxides the calculated ionization energies are intermediate between those of the corresponding hexachloride and nitrido-species, reflecting the overall trend of the electrochemical data. Comparison between metals is not so successful (Table 4). The calculated ionization energy of $[MoCl_6]^-$ is the highest of the systems studied, in line with its extreme oxidation potential and the ionization energies are higher for $[MoX_6]^-$ than for $[WX_6]^-$ (X = F or Cl), reflecting the experimental observation of more positive electrode potentials in the molybdenum systems. However, the difference is small compared to shifts in E° data and the higher oxidation potentials of

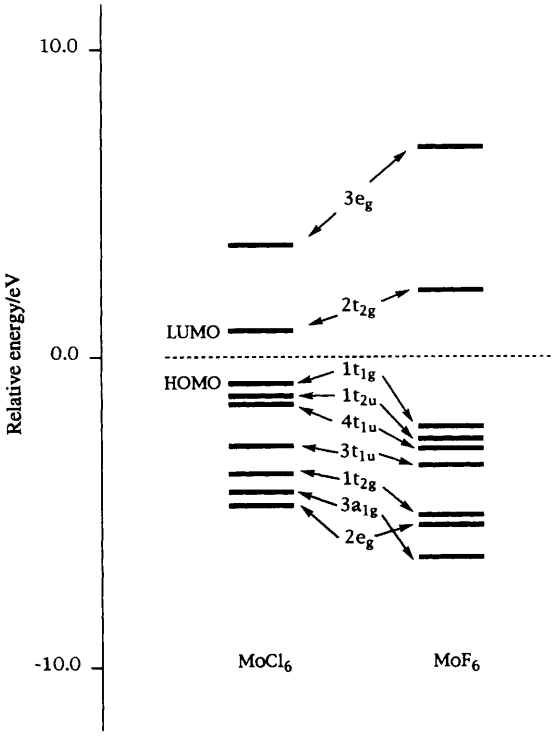

Fig. 8 Molecular orbital diagrams for $MoCl_6$ and MoF_6. Energies are relative with zero energy set to be the midpoint of the HOMO – LUMO gap

the substituted molybdenum species relative to their tungsten analogues are not reflected in the calculated ionization energies of those species. As a result we shall not attempt any comparison between the two different metal series, but limit ourselves to a discussion of trends observed within one metal series. We have chosen the molybdenum systems as more structural data are available. However, as similar trends have been calculated for the tungsten analogues any conclusions should apply to these systems as well.

$MoCl_6$ *versus* MoF_6. The electronic structure of regular octahedral species is well known.[49] Fig. 8 compares the relative energies of the frontier molecular orbitals of $MoCl_6$ and MoF_6. The metal d orbitals are split by the interaction with the ligand orbitals to produce the familiar t_{2g} and e_g orbitals. For the hexahalide species the metal-based $2t_{2g}$ orbitals have some antibonding character due to a π interaction with the occupied halide-based orbitals. For a d^1 species a single electron is located in this t_{2g} level. To lower energy lie four halide-based orbitals, non-bonding with respect to the metal, and the M–X bonding orbitals, $1t_{2g}$, $3a_{1g}$ and $2e_g$. One obvious difference between the fluoride and chloride MO schemes is the much larger gap between the $2t_{2g}$ orbital and the ligand-based $1t_{1g}$ orbital for the fluoride. This is a consequence of the much lower energy of the F^- donor orbitals compared to those of Cl^-. The larger energy mismatch results in a greater degree of metal character in the $2t_{2g}$ orbital of MoF_6 than in that of $MoCl_6$. On this basis alone, one might expect oxidation to the d^0 species to be easier for the chloride as the orbital involved displays more M–X antibonding character. That this is not observed experimentally suggests a deeper analysis is required, as follows.

To understand the different electrochemical data observed for MoF_6 and $MoCl_6$ we make use of an energy-decomposition scheme[50] to analyse the bonding between the $[X_6]^{6-}$ ligand array and the central metal ion (Mo^{6+} or Mo^{5+}) in the hypothetical reaction $Mo^{n+} + [X_6]^{6-} \longrightarrow [MoX_6]^{(6-n)-}$. The results of this fragment analysis are presented in Table 5. The computed total energies show that both d^0 and d^1 metal centres are significantly more stabilized by $[F_6]^{6-}$ than by $[Cl_6]^{6-}$. This is due to the greater electrostatic interaction

Table 5 Energy-decomposition analysis (eV) for $[MoX_6]^-$ and MoX_6 (X = F or Cl)[a]

	$MoCl_6$	$[MoCl_6]^-$	MoF_6	$[MoF_6]^-$
Steric interaction:				
Pauli repulsion	+19.1	+17.6	+24.8	+22.3
Electrostatic interaction	−182.9	−152.4	−253.4	−208.0
Total steric interaction	−163.7	−134.8	−228.6	−185.8
Orbital interaction:				
a_{1g}	−4.8	−3.8	−2.8	−2.2
e_g	−38.9	−28.8	−27.0	−19.8
t_{2g}	−44.2	−25.4	−31.3	−19.8
Total orbital interaction	−109.2	−73.4	−77.2	−53.4
Total energy:[b]				
$M^{n+} + [X_6]^{6-} \longrightarrow [MX_6]^{(6-n)-}$	−270.0	−205.5	−302.4	−236.0

[a] The total bonding energy between two fragments can be broken up into terms for steric repulsion and orbital interaction. The steric repulsion term is made up of four-electron destabilization between occupied orbitals (Pauli repulsion) and an electrostatic term due to the interaction between the electronic and nuclear charge distributions on the two fragments. The orbital interaction term can also be further partitioned into contributions from each irreducible representation [50]. For Mo^{5+} a restricted calculation was performed in O_h symmetry with the single d electron placed in a t_{2g} orbital. [b] Becke–Perdew corrections included in calculation of total energy term.

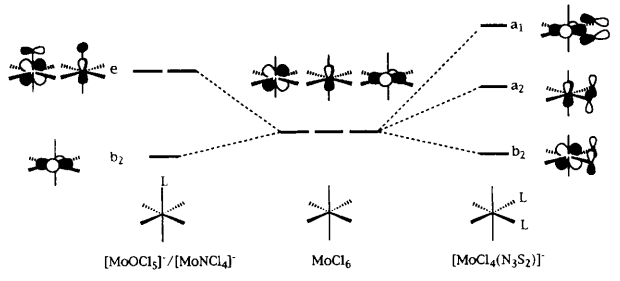

Fig. 9 Splitting of octahedral t_{2g} orbitals upon substitution

between the $[F_6]^{6-}$ moiety and the metal centre. This term is dominant, although it is offset by the greater orbital interaction seen for the chloride, arising from the smaller energy mismatch between halide donor and metal acceptor orbitals as discussed above. For both halides, orbital interactions are greater in the d^0 systems, in particular within t_{2g} symmetry. The shortening of the M–X bond upon oxidation results in better orbital overlap and accounts for the general calculated increase. This effect is reinforced within t_{2g} symmetry as an antibonding electron is removed and is larger for the chloride system due to the higher degree of antibonding character of the $2t_{2g}$ orbital. Overall, the greater ability of F^- to stabilize high oxidation states results from a higher electrostatic interaction between the metal and the ligand array for this halide and is responsible for MoF_6 being relatively more accessible electrochemically than is $MoCl_6$.

Comparison of substituted d^1 species with $[MoCl_6]^-$. The electrochemical data demonstrate that the ease of oxidation of the d^1 systems is crucially dependent on the nature of the ligands present. This overall trend is reproduced by the calculated ionization energies and reflects a large variation in the energy of the electroactive orbital. In all cases the orbital involved is related to one of the π-antibonding $2t_{2g}$ sets of the regular octahedron which, upon substitution, is split in energy through the different π-donor abilities of the new ligands, L. These new π interactions are shown schematically in Fig. 9. For $[MoOCl_5]^{2-}$ and $[MoNCl_4]^{2-}$ (C_{4v} symmetry) the single d electron occupies a b_2 orbital lying in the pseudo-$\{MoCl_4\}$ plane. To higher energy is an e pair, destabilized through π interaction with the axial ligands. That this pair lies to higher energy than the b_2 orbital suggests that L (O or N) is a stronger π donor than is Cl^-. For $[MoCl_4(N_3S_2)]^{2-}$ (C_{2v} symmetry) the octahedral $2t_{2g}$ set splits to give a singly occupied b_2 orbital with a_1 and a_2 orbitals to higher energy. For $[MoOCl_5]^{2-}$ and $[MoNCl_4]^{2-}$ the axial ligands do not have any direct interaction with the electroactive b_2 orbital and the energy of this orbital will only be directly affected by π destabilization from the Cl^- ligands of the pseudo-$\{MoCl_4\}$ plane. Allowing for the slight variations in geometry, this $\{MoCl_4\}$ moiety is common to both $[MoOCl_5]^{2-}$ and $[MoNCl_4]^{2-}$ as well as the parent hexachloride species. In these three systems calculated Mo–Cl distances within this fragment range from 2.309 to 2.350 Å and from 2.348 to 2.438 Å for the d^0 and d^1 systems respectively. Therefore one would not expect the large shifts in $E°$ data to result simply from variation in π donation within the $\{MoCl_4\}$ unit. The energy of this in-plane orbital is clearly dependent on the nature of the axial ligands, despite no direct orbital interaction with them. We must therefore consider another mechanism by which the axial ligands dictate the relative energies of the electroactive orbital. In a similar way we can compare $[MoCl_4(N_3S_2)]^{-/2-}$ with $[MoCl_6]^{0/-}$ by noting that these species contain a common C_{2v} $\{MoCl_4\}$ unit. Comparison of the optimized geometries of these species again suggests that there is little variation in the electronic structure of this fragment. In this case, however, the electroactive b_2 orbital will undergo a direct interaction with two *cis* substituents (either two Cl^- ligands or the $\{N_3S_2\}^{3-}$ moiety) and this interaction must be taken into account in the discussion of these systems.

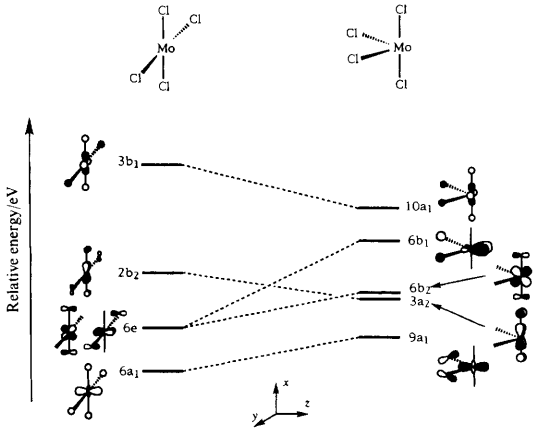

Fig. 10 Acceptor orbitals of square-planar and bent $\{MoCl_4\}^{2+}$ fragments of $MoCl_6$. Symmetry labels are those adopted in the text: C_{4v} and C_{2v} for square-planar and bent geometries respectively

To understand the variation in energy of the electroactive b_2 orbital we again resort to fragment analyses. Our first series of calculations will study the interaction of the axial ligands, L^{ax} (*trans*-$\{Cl\cdots Cl\}^{2-}$, *trans*-$\{O\cdots Cl\}^{3-}$ and N^{3-}) with the C_{4v} $\{MoCl_4\}^{2+}$ moiety as it is found in the optimized structures of $MoCl_6$, $[MoOCl_5]^-$ and $[MoNCl_4]^-$ respectively. We then compare the interaction between the equatorial substituents,

Table 6 d-Orbital occupations of C_{4v} $\{MoCl_4\}^{2+}$ fragments of $MoCl_6$, $[MoOCl_5]^-$ and $[MoNCl_4]^-$

	Occupation		
Orbital	$MoCl_6$	$[MoOCl_5]^-$	$[MoNCl_4]^-$
d_{xy}	0.86	0.86	0.84
d_{xz}, d_{yz}	1.05	0.97	0.89
d_{z^2}	0.39	0.39	0.60
$d_{x^2-y^2}$	0.90	0.90	0.89

L^{eq} (*cis*-$\{Cl\cdots Cl\}^{2-}$ and $[N_3S_2]^{3-}$) and the C_{2v} $\{MoCl_4\}^{2+}$ fragment in $MoCl_6$ and $[MoCl_4(N_3S_2)]^-$. The geometries and electron occupations of the optimized d^0 systems will be used.

The acceptor orbitals of planar and bent $\{MoCl_4\}^{2+}$ fragments are well known and are displayed in Fig. 10.[49,51] The degeneracy of the octahedral t_{2g} and e_g orbitals is split by the removal of two ligands, with, in the C_{4v} case, the $6a_1$ and 6e orbitals stabilized relative to the in-plane $2b_2$ and $3b_1$ orbitals which are effectively unchanged from the octahedron. The $6a_1$ and 6e orbitals will act as σ- and π-acceptors respectively for the interaction with L^{ax}. In the C_{2v} $\{MoCl_4\}^{2+}$ fragment all five metal-based orbitals may potentially act as acceptor orbitals.

$MoCl_6$ *versus* $[MoOCl_5]^-$ and $[MoNCl_4]^-$. Before proceeding, it is worthwhile testing our assumption that variation in the geometry of the C_{4v} $\{MoCl_4\}^{2+}$ fragment as is found in these species does not result in significant changes to its electronic structure. This can be done by monitoring the occupations of the molybdenum d orbitals within this fragment (see Table 6). Most importantly, only minor variation is seen in the occupation of the in-plane d_{xy} orbital, which corresponds to the electroactive orbital in the final molecule. Similarly, little variation in occupancy is calculated for the $d_{x^2-y^2}$ orbital. The increasing occupation of the d_{z^2} orbital in $[MoOCl_5]^-$ and $[MoNCl_4]^-$ is due to the deformation of the $\{MoCl_4\}$ moiety resulting in the onset of π donation into this orbital. The higher d_{z^2} occupation is offset by a loss of π donation into the d_{xz} and d_{yz} orbitals under the same deformation. Similar effects have been found in distorted ML_5 systems.[52] Overall our assumption of a constant C_{4v} $\{MoCl_4\}^{2+}$ fragment in these systems seems secure.

Table 7 gives the occupations of the $6a_1$ and 6e acceptor orbitals of the C_{4v} $\{MoCl_4\}^{2+}$ fragment in $MoCl_6$, $[MoOCl_5]^-$ and $[MoNCl_4]^-$. These orbital occupations show that considerable variation in donor power occurs in going from L^{ax} = *trans*-$\{Cl\cdots Cl\}^{2-}$ to *trans*-$\{O\cdots Cl\}^{3-}$ and finally N^{3-}. Nitride is the strongest donor, in terms of both its σ- and π-abilities. Within this series *trans*-$\{O\cdots Cl\}^{3-}$ displays intermediate π donation while it is a comparable σ donor to *trans*-$\{Cl\cdots Cl\}^{2-}$. This last fragment is the weakest π donor. These conclusions are reinforced by the orbital interactions in a_1 and e symmetry which give a measure of the extent of σ- and π-donation respectively from L^{ax} to C_{4v} $\{MoCl_4\}^{2+}$ (Table 8). The total orbital interactions (which include small contributions from other symmetries) underline the conclusion that the donor power increases markedly in the order *trans*-$\{Cl\cdots Cl\}^{2-}$ < *trans*-$\{O\cdots Cl\}^{3-}$ < N^{3-}.

This analysis has highlighted a strong correlation between the ease of formation of the d^0 species (low oxidation potential, low calculated ionization energy) and the extent of donation from L^{ax}. The axial ligand does not directly interact with the b_2 orbital but affects the energy of that orbital by the degree of electron donation to the metal. The stronger the donor power of L^{ax} the more electron density builds up at the metal, destabilizing all metal-based orbitals, including the electroactive b_2 orbital.

These trends can be understood if we consider the nature of the donor orbitals of L^{ax}. Comparing N to O one would expect the valence orbitals of the former to be both higher in energy and more diffuse, leading to stronger interaction with the C_{4v} $\{MoCl_4\}^{2+}$ acceptor orbitals through both better energy matching and overlap. These factors are so significant that N^{3-} remains a better overall donor than the combination of O^{2-} and Cl^- ligands. The comparison between N^{3-} and two Cl^- ligands is not so straightforward as we move down one row in the Periodic Table and to the right. The computed overlap between the $6a_1$ acceptor orbital of C_{4v} $\{MoCl_4\}^{2+}$ and the a_1 donor orbitals of N^{3-} and *trans*-$\{Cl\cdots Cl\}^{2-}$ is in fact higher for the latter (0.23 *vs* 0.37). The increased σ-donor capacity of N^{3-} must therefore arise from a significantly better energy match with the C_{4v} $\{MoCl_4\}^{2+}$ acceptor orbitals. This in turn may result from the high density of negative charge on this relatively small ligand. The better energy match will also increase π donation from N^{3-} relative to *trans*-$\{Cl\cdots Cl\}^{2-}$. However, in this case the overlap between the C_{4v} $\{MoCl_4\}^{2+}$ 6e acceptor orbitals and the ligand donor orbital is much higher for N^{3-} (0.21 *vs* 0.03) resulting in the overall increase in π donation between N^{3-} and *trans*-$\{Cl\cdots Cl\}^{2-}$ being greater than that seen for σ donation. This better overlap is probably a result of the deformation of the C_{4v} $\{MoCl_4\}^{2+}$ unit which results in the onset of a σ-antibonding interaction between each of the C_{4v} $\{MoCl_4\}^{2+}$ e pair with two *trans* Cl^- ligands. These acceptor orbitals are thus hybridized towards the N^{3-} ligand, improving the overlap with its donor orbitals.[52] This variation in energy of the donor orbitals of L^{ax} and the different overlap with the metal fragment orbitals result in the low oxidation potential of the $[MoNCl_4]^{-/2-}$ couple (N^{3-} a strong donor) and the relatively high positive potential of the $[MCl_6]^{0/-}$ oxidation (*trans*-$\{Cl\cdots Cl\}^{2-}$ a poor donor).

Table 7 The C_{4v} $\{MoCl_4\}^{2+}$ acceptor orbital occupations in $MoCl_6$, $[MoOCl_5]^-$ and $[MoNCl_4]^-$

	Occupation		
Orbital	$MoCl_6$	$[MoOCl_5]^-$	$[MoNCl_4]^-$
6e	0.50	0.90	1.04
$6a_1$	0.69	0.65	0.86

Table 8 Orbital interaction energies (eV) between C_{4v} $\{MoCl_4\}^{2+}$ and L^{ax} in $MoCl_6$, $[MoOCl_5]^-$ and $[MoNCl_4]^-$

	Interaction energy		
Orbital symmetry	$MoCl_6$	$[MoOCl_5]^-$	$[MoNCl_4]^-$
$a_1(\sigma)$	−4.8	−7.4	−11.8
$e(\pi)$	−4.5	−15.5	−23.8
Total	−11.1	−23.7	−37.5

Table 9 d-Orbital occupations of C_{2v} $\{MoCl_4\}^{2+}$ fragments in $MoCl_6$ and $[MoCl_4(N_3S_2)]^-$

	Occupation	
Orbital	$MoCl_6$	$[MoCl_4(N_3S_2)]^-$
d_{z^2}	0.74	0.73
$d_{x^2-y^2}$	0.85	0.83
d_{xy}	0.77	0.80
d_{xz}	0.81	0.80
d_{yz}	0.79	0.82

$[MoCl_6]^-$ *versus* $[MoCl_4(N_3S_2)]^{2-}$. Table 9 gives the molybdenum d-orbital occupations of the C_{2v} $\{MoCl_4\}^{2+}$ moiety as are found within $MoCl_6$ and $[MoCl_4(N_3S_2)]^-$. There is very little variation in occupation confirming our assumption of a constant C_{2v} $\{MoCl_4\}^{2+}$ fragment in these species.

The C_{2v} $\{MoCl_4\}^{2+}$ acceptor-orbital occupations in $MoCl_6$ and $[MoCl_4(N_3S_2)]^-$ are given in Table 10 and indicate that the $\{N_3S_2\}^{3-}$ moiety donates substantially more electron density to the metal fragment than do two Cl^- ligands in a

Table 10 The C_{2v} $\{MoCl_4\}^{2+}$ acceptor-orbital occupations in $MoCl_6$ and $[MoCl_4(N_3S_2)]^-$

	Occupation	
Orbital	$MoCl_6$	$[MoCl_4(N_3S_2)]^-$
$9a_1$	0.43	0.55
$10a_1$	0.29	0.29
$3a_2$	0.22	1.11
$6b_1$	0.55	0.65
$6b_2$	0.25	0.25

Table 11 Orbital interaction energies (eV) between C_{2v} $\{MoCl_4\}^{2+}$ and L^{eq} in $MoCl_6$ and $[MoCl_4(N_3S_2)]^-$

	Interaction energy	
Orbital symmetry	$MoCl_6$	$[MoCl_4(N_3S_2)]^-$
a_1	−5.0	−7.9
a_2	−1.4	−6.8
b_1	−4.7	−7.5
b_2	−1.4	−2.7
Total	−12.4	−24.8

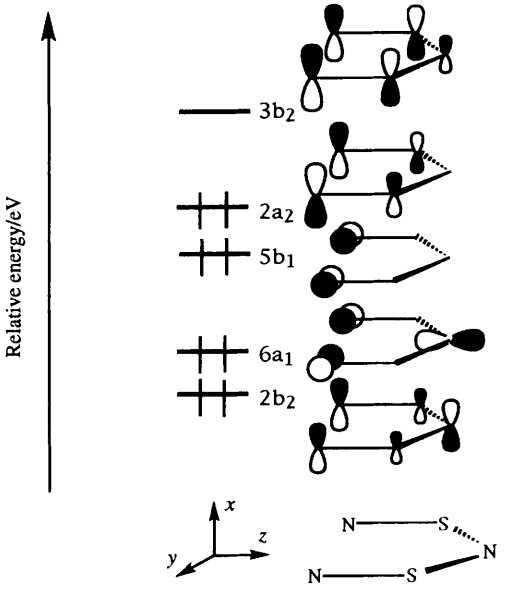

Fig. 11 Frontier molecular orbitals of the $\{N_3S_2\}^{3-}$ moiety

cis arrangement. All five acceptor orbitals exhibit higher occupations in $[MoCl_4(N_3S_2)]^-$, although the effect is largest for the a_2 orbital. This overall trend is also evident in the orbital-interaction energies (Table 11), again the biggest difference being within a_2 symmetry. The b_2 orbital interaction is larger in $[MoCl_4(N_3S_2)]^-$ and this would be expected to raise the energy of the b_2 LUMO in this species compared to its counterpart in $MoCl_6$. However, the b_2 orbital occupation is barely higher in $[MoCl_4(N_3S_2)]^-$ than in $MoCl_6$. This is because the $\{N_3S_2\}^{3-}$ moiety also has a low-lying b_2 acceptor orbital which can stabilize the b_2 LUMO *via* Mo–N back donation (see Fig. 11).* The oxidation potentials of the $[MoCl_6]^{0/-}$ and $[MoCl_4(N_3S_2)]^{-/2-}$ couples are again reflections of the total donation from L^{eq}. The total orbital interaction between C_{2v} $\{MoCl_4\}^{2+}$ and $\{N_3S_2\}^{3-}$ is twice that calculated between C_{2v} $\{MoCl_4\}^{2+}$ and *cis*-$\{Cl\cdots Cl\}^{2-}$. Comparison of the computed orbital overlap between acceptor and donor orbitals within these two systems indicates that only small differences occur. The much stronger donor power of the $\{N_3S_2\}^{3-}$ moiety must therefore be a result of the higher energy of its donor orbitals. This is particularly the case for the a_2 donor orbital, the HOMO of the $\{N_3S_2\}^{3-}$ moiety, which is an antibonding orbital in the ring π system. Donation from this orbital is particularly efficient and this probably lies behind the non-observation of a ligand-based oxidation in the metallacycle system whereas the isolated dithiatriazene ligand is readily oxidized.[28]

Experimental

Starting materials and general procedures

The compounds WCl_6 and $MoCl_5$ (Aldrich) were freed from chloride oxide impurities by fractional sublimation in a sealed Pyrex tube using a three-zone tube furnace; $[NBu_4][MoCl_6]$,[8] $[NBu_4]_2[MoCl_6]$,[9] $[NBu_4][WCl_6]$,[10] $[NBu_4]_2[MoOCl_5]$,[9] $[NBu_4]_2[WOCl_5]$,[9] $[AsPh_4][MoNCl_4]$,[11] $[AsPh_4][WNCl_4]$,[11] $[AsPh_4][MoCl_4(N_3S_2)]$,[12] $[AsPh_4][WCl_4(N_3S_2)]$,[13] $[MoCl_3\{N_2(PPh_2)N\}]$[14] and $[WCl_3\{N_2(PPh_2)N\}]$[15] were prepared by the literature methods.

* The orbital which has this topology in the metallaphosphazenes (identified as π_2 in Fig. 2 of ref. 26) lies much higher in energy. We feel that this difference explains the greater stabilization of high-oxidation-state metals by $[N_2(PPh_2)_2N]^{3-}$ than by $[N_3S_2]^{3-}$, which are otherwise very similar ligands.

Electrochemistry

Cyclic voltammetric studies (scan rates ν = 20–10 000 mV s^{-1}) and phase-sensitive alternating current (a.c.) measurements (ω = 615 Hz, ν = 10 mV s^{-1}) were made with a PAR 173 potentiostat in combination with a PAR 175 programmer and EG&G 9209 lock-in amplifier and recorded on a Houston Graphics 2000 XY plotter or on a Hewlett-Packard 181 storage oscilloscope. Electrochemical experiments were performed on a platinum three-electrode system with the working electrode either a wire or a 0.5 mm diameter micro-tip. The vacuum-tight all-glass cell has been described in detail elsewhere.[3a] The electrolyte NBu_4PF_6 (Aldrich) was placed in the electrochemical cell and dried under vacuum at 373 K for 16 h. Then the solvent, dry degassed CH_2Cl_2, was vacuum-transferred into the cell. Samples and ferrocene as an internal reference were added to the cell using break-seal techniques. The ferrocenium–ferrocene couple appeared in this system at +0.48 (CH_2Cl_2) V *vs.* SCE at 298 K.

Computational details

Calculations employed the Amsterdam density functional (ADF) package developed by Baerends *et al.*[53] and employed the numerical integration scheme of te Velde and co-workers.[54] Triple-ζ STO (Slater-type orbital) basis sets were employed for Mo and W and double-ζ STO basis sets extended with a polarization function for all other atoms.[55] An auxiliary set of s, p, d, f and g STO basis functions centred on all nuclei was used in order to fit the molecular density and describe accurately the coulomb and exchange potentials in each self-consistent field (SCF) cycle.[56] Core electrons (up to and including 3d for Mo, 5p for W, 2p for Cl and S and 1s for O and N) were treated using the frozen-core approximation. The local density approximation[57] (LDA) was employed using the parametrization of Vosko *et al.*[58] Geometry optimization was performed using the method developed by Versluis and Ziegler.[59] The energies of all LDA-optimized species were recalculated to include the non-local gradient corrections of Becke[60] and Perdew[61] as well as the quasi-relativistic correction of Ziegler *et al.*[62] Spin-polarized, unrestricted calculations were performed on all open-shell d^1 species.

Acknowledgements

This work was supported by the Natural Sciences and

Engineering Research Council of Canada through an operating grant (to R. T. B.) and by the University of Lethbridge Research Fund. K. H. M. thanks the Alexander von Humboldt Foundation for a Feodor Lynen Fellowship, and Dr. R. Stranger for the use of extra computing facilities at the Australian National University.

References

1 W. A. Herrmann, R. Serrano and H. Bock, *Angew. Chem., Int. Ed. Engl.*, 1984, **23**, 383.
2 G. Hogarth, P. C. Konidaris and G. C. Saunders, *J. Organomet. Chem.*, 1991, **406**, 153.
3 (*a*) K. H. Moock and M. H. Rock, *J. Chem. Soc., Dalton Trans.*, 1993, 2459; (*b*) G. M. Anderson, J. Iqbal, D. W. A. Sharp, J. M. Winfield, J. H. Cameron and A. G. McLeod, *J. Fluorine Chem.*, 1984, **24**, 303.
4 (*a*) G. A. Heath, G. T. Hefter, T. W. Boyle, C. D. Desjardin and D. W. A. Sharp, *J. Fluorine Chem.*, 1978, **11**, 399; (*b*) S. Brownstein, G. A. Heath, A. Sengupta and D. W. A. Sharp, *J. Chem. Soc., Chem. Commun.*, 1983, 669.
5 G. A. Heath, K. H. Moock, D. W. A. Sharp and L. J. Yellowlees, *J. Chem. Soc., Chem. Commun.*, 1985, 1503.
6 W. M. Latimer, *Oxidation Potentials*, 2nd edn., Prentice-Hall, Englewood Cliffs, NJ, 1952.
7 H. W. Roesky, J. Anhaus, H. G. Schmidt, G. M. Sheldrick and M. Noltemeyer, *J. Chem. Soc., Dalton Trans.*, 1983, 1207.
8 B. J. Brisdon and R. A. Walton, *J. Inorg. Nucl. Chem.*, 1965, **27**, 1101.
9 J. A. Creighton and T. J. Sinclair, *Spectrochim. Acta, Part A*, 1979, **35**, 507.
10 R. N. Dickenson, S. E. Feil, F. N. Collier, W. W. Horner, S. M. Horner and S. Y. Tyree, *Inorg. Chem.*, 1964, **3**, 1600.
11 K. Dehnicke and W. Kolitsch, *Z. Naturforsch., Teil B*, 1977, **32**, 1485.
12 J. Anhaus, P. G. Jones, M. Noltemeyer, W. Pinkert, H. W. Roesky and G. M. Sheldrick, *Inorg. Chim. Acta*, 1985, **97**, L7.
13 H. Wadle, E. Conradi, U. Müller and K. Dehnicke, *Z. Naturforsch, Teil B*, 1985, **40**, 1626.
14 H. W. Roesky, K. V. Katti, U. Seseke, H. G. Schmidt, E. Egert, R. Herbst and G. M. Sheldrick, *J. Chem. Soc., Dalton Trans.*, 1987, 847.
15 H. W. Roesky, K. V. Katti, U. Seseke, M. Witt, E. Egert, R. Herbst and G. M. Sheldrick, *Angew. Chem.*, 1986, **98**, 447; *Angew. Chem., Int. Ed. Engl.*, 1986, **25**, 477.
16 H. F. Hagedorn, R. T. Iwamoto and J. Kleinberg, *J. Electroanal. Chem. Interfacial Electrochem.*, 1973, **46**, 307.
17 M. Gilet, A. Mortreux, J.-C. Folest and F. Petit, *J. Am. Chem. Soc.*, 1983, **105**, 3876.
18 O. Piovesana, *Gazz. Chim. Ital.*, 1969, **99**, 86.
19 H. W. Roesky, T. Tojo, M. Ilemann and D. Westhoff, *Z. Naturforsch., Teil B*, 1987, **42**, 877.
20 G. A. Heath and J. E. McGrady, *J. Chem. Soc., Dalton Trans.*, 1994, 3759.
21 T. Ziegler, *Chem. Rev.*, 1991, **91**, 651; *Density Functional Theory of Many Electron Systems*, eds. E. S. Kryachko and E. V. Ludena, Kluwer, Dordrecht, 1990; T. Ziegler and L. Fan, *J. Chem. Phys.*, 1991, **95**, 7401.
22 (*a*) M. A. Buijse and E. J. Baerends, *J. Chem. Phys.*, 1990, **93**, 4129; (*b*) G. L. Gutsev and A. I. Boldyrev, *Mol. Phys.*, 1984, **53**, 23; *Chem. Phys. Lett.*, 1983, **101**, 441; *J. Phys. Chem.*, 1990, **94**, 2256; (*c*) C. Sosa, J. Andzelm, B. C. Elkin, E. Wimmer, K. D. Dobbs and D. A. Dixon, *J. Phys. Chem.*, 1992, **96**, 6630; (*d*) R. J. Deeth, *J. Chem. Soc., Dalton Trans.*, 1995, 1537; (*e*) P. D. Lyne and D. M. P. Mingos, *J. Chem. Soc., Dalton Trans.*, 1995, 1635; (*f*) T. Ziegler and J. Li, *Organometallics*, 1995, **14**, 214; (*g*) A. Neuhaus, A. Feldkamp and G. Frenking, *Inorg. Chem.*, 1994, **33**, 5278.
23 Y. Sakai and E. Miyoshi, *J. Chem. Phys.*, 1987, **87**, 2885; E. Miyoshi, Y. Sakai, A. Murakami, H. Iwaki, H. Terashima, T. Shoda and T. Kawaguchi, *J. Chem. Phys.*, 1988, **89**, 4193.
24 M. Gutowski, J. Rak, P. Dokurno and J. Blazejowski, *Inorg. Chem.*, 1994, **33**, 6187.
25 R. T. Boeré and K. H. Moock, *J. Am. Chem. Soc.*, 1995, **117**, 4755.
26 R. T. Boeré, V. Klassen and K. H. Moock, *Phosphorus Sulfur Silicon Relat. Elem.*, 1994, **93–94**, 249.
27 E. A. Allen, B. J. Brisdon and G. W. A. Fowles, *J. Chem. Soc.*, 1964, 4531.
28 R. T. Boeré, J. Fait, K. Larsen and J. Yip, *Inorg. Chem.*, 1992, **31**, 1417; R. T. Boeré, C. L. French, R. T. Oakley, A. W. Cordes, J. A. J. Privett, S. L. Craig and J. B. Graham, *J. Am. Chem. Soc.*, 1985, **107**, 7710; R. T. Boeré, R. T. Oakley and M. Shevalier, *J. Chem. Soc., Chem. Commun.*, 1987, 110; N. Burford, T. Chivers, R. T. Oakley and T. Oswald, *Can. J. Chem.*, 1984, **62**, 712; R. Maggiulli, R. Mews, W. D. Stohrer, M. Noltemeyer and G. M. Sheldrick, *Chem. Ber.*, 1988, **121**, 1881.
29 R. J. Gillespie, *J. Chem. Educ.*, 1970, **47**, 18.
30 J. H. Levy, P. L. Sanger, J. C. Taylor and P. W. Wilson, *Acta Crystallogr., Sect. B*, 1975, **31**, 1065.
31 J. H. Levy, J. C. Taylor and P. W. Wilson, *J. Less-Common Met.*, 1974, **45**, 155.
32 J. A. A. Ketelaar and G. W. Van Oosterhout, *Recl. Trav. Chim. Pays-Bas*, 1943, **62**, 197.
33 D. E. Sands and A. Zalkin, *Acta Crystallogr.*, 1959, **12**, 723.
34 W. Eichler and H.-J. Seifert, *Z. Anorg. Allg. Chem.*, 1977, **431**, 123.
35 U. Kynast, E. Conradi, U. Müller and K. Dehnicke, *Z. Naturforsch., Teil B*, 1984, **39**, 1680.
36 S. A. Macgregor, G. A. Heath and K. H. Moock, unpublished work.
37 J. E. Bloor and R. E. Sherrod, *J. Am. Chem. Soc.*, 1980, **102**, 4333.
38 R. N. Compton, P. W. Reinhardt and C. D. Cooper, *J. Chem. Phys.*, 1978, **68**, 2023; J. Burgess, I. Haigh, R. D. Peacock and P. Taylor, *J. Chem. Soc., Dalton Trans.*, 1974, 1064; L. N. Sidorov, A. Y. Borshchevsky, E. B. Rudny and V. D. Butsky, *Chem. Phys.*, 1982, **71**, 145; L. N. Sidorov, *Usp. Khim.*, 1982, **51**, 625.
39 C. K. Jørgensen, in *Halogen Chemistry*, ed. V. Gutman, Academic Press, London and New York, 1967, vol. 1, pp. 293–401.
40 D. Brown, *J. Chem. Soc.*, 1964, 4944; A. Sabatini and I. Bertini, *Inorg. Chem.*, 1966, **5**, 204.
41 W. Kolitsch and K. Dehnicke, *Z. Naturforsch., Teil B*, 1970, **25**, 1080.
42 B. Knopp, K.-P. Lörcher and J. Strähle, *Z. Naturforsch., Teil B*, 1977, **32**, 1361; U. Müller, E. Schwenda and J. Strähle, *Z. Naturforsch., Teil B*, 1983, **38**, 1299.
43 *Gmelin Handbook*, Mo Suppl., 1990, vol. 5, B5, pp. 386–389.
44 P. Pyykkö, *Chem. Rev.*, 1988, **88**, 563.
45 J. Schmitte, C. Friebel, F. Weller and K. Dehnicke, *Z. Anorg. Allg. Chem.*, 1982, **495**, 148.
46 A. Bino and F. A. Cotton, *J. Am. Chem. Soc.*, 1979, **101**, 4150.
47 U. Weiher, K. Dehnicke and D. Fenske, *Z. Anorg. Allg. Chem.*, 1979, **457**, 105.
48 I. W. Bassi and R. Scordamaglia, *J. Organomet. Chem.*, 1975, **99**, 127.
49 T. A. Albright, J. K. Burdett and M.-H. Whangbo, *Orbital Interactions in Chemistry*, Wiley, New York, 1985.
50 T. Ziegler, *NATO ASI, Ser. C*, 1992, **378**, 367.
51 M. Elian and R. Hoffmann, *Inorg. Chem.*, 1975, **14**, 1058.
52 A. R. Rossi and R. Hoffmann, *Inorg. Chem.*, 1975, **14**, 365.
53 E. J. Baerends, D. E. Ellis and P. Ros, *Chem. Phys.*, 1973, **2**, 41; E. J. Baerends, J. G. Snijders, C. A. de Lange, and G. Jonkers, *Local Density Approximations in Quantum Chemistry and Solid State Physics*, eds. J. P. Dahl and J. Avery, Plenum, New York, 1984.
54 P. M. Boerrigter, G. te Velde and E. J. Baerends, *Int. J. Quantum Chem.*, 1988, **33**, 87.
55 G. J. Snijders, E. J. Baerends and P. Vernooijs, *At. Data Nucl. Data Tables*, 1982, **26**, 483; P. Vernooijs, G. J. Snijders and E. J. Barends, *Slater Type Basis Functions for the whole Periodic System*, Internal Report, Free University of Amsterdam, 1981.
56 J. Krijn and E. J. Baerends, *Fit Functions in the HFS-method*, Internal Report, Free University of Amsterdam, 1984.
57 O. Gunnarsson, B. I. Lundquist and J. W. Wilkins, *Phys. Rev. B*, 1974, **10**, 1319; O. Gunnarson and B. I. Lundquist, *Phys. Rev. B*, 1974, **13**, 4274; O. Gunnarsson, M. Johnson and B. I. Lundquist, *Phys. Rev. B*, 1979, **20**, 3136.
58 S. H. Vosko, L. Wilk and M. Nusair, *Can. J. Phys.*, 1980, **58**, 1200.
59 L. Versluis and T. Ziegler, *J. Chem. Phys.*, 1988, **88**, 322.
60 A. D. Becke, *J. Chem. Phys.*, 1986, **84**, 4524.
61 J. P. Perdew, *Phys. Rev. B*, 1986, **33**, 8822.
62 T. Ziegler, V. Tschinke, E. J. Baerends, J. G. Snijders and W. Ravenek, *J. Phys. Chem.*, 1989, **93**, 3050.

Received 20*th October* 1995; *Paper* 5/06931I